25th ABCM International Congress of Mechanical Engineering
October 20-25, 2019, Uberlândia, MG, Brazil

COB-2019-1506
ACTUATOR AND SENSOR PLACEMENT FOR CLOSED-LOOP CONTROL OF CONVECTIVE INSTABILITIES. PART 1: 2D TOLLMIEN-SCHLICHTING WAVES

Guilherme A. Freire
André V. G. Cavalieri
Flávio J. Silvestre
Instituto Tecnológico de Aeronáutica
gafreire0@gmail.com, andre@ita.br, flaviojs@ita.br

A. Hanifi
D. S. Henningson
Royal Institute of Technology
hanifi@kth.se, henning@kth.se

Abstract. *This work deals with the characterization of the closed-loop control performance aiming at the delay of transition. We focus on convective wavepackets, typical of the initial stages of transition to turbulence, starting with the linearized Kuramoto-Sivashinsky equation as a model problem representative of the transitional 2D boundary layer; its simplified structure and reduced order provide a manageable framework for the study of fundamental concepts involving the control of linear wavepackets. The characterization is then extended to the 2D Blasius boundary layer. The objective of this study is to explore how the sensor-actuator placement affects the optimal control problem, formulated using linear quadratic gaussian (LQG) regulators. This is carried out by evaluating errors of the optimal estimator at positions where control gains are significant, through a proposed metric, labelled as γ. Results show, in quantitative manner, why some choices of sensor-actuator placement are more effective than others for flow control: good (respectively bad) closed-loop performance is obtained when estimation errors are low (respectively high) in the regions with significant gains in the full-state-feedback problem. Unsatisfactory performance is further understood as dominant estimation error modes that overlap spatially with control gains, which shows directions for improvement of a given setup by moving sensors or actuators. The proposed metric and analysis explain most trends in closed-loop performance as a function of sensor and actuator position, obtained for the model problem and for the 2D Blasius boundary layer. The spatial characterization of the γ-metric provides thus a valuable and intuitive tool for the problem of sensor-actuator placement.*

Keywords: *Convective instabilities, Closed-loop control, Sensor-actuator placement*

1. INTRODUCTION

Closed-loop flow control is a strategy that combines the open-loop dynamics of the governing equations, given by stability theory, and the input-output approach of control theory, aiming at the manipulation of the system behavior (Bagheri *et al.*, 2009b). One of its most prominent objectives is the control of instabilities in the boundary layer over a wing to delay transition to turbulence and thus reduce the skin friction drag (Schrauf, 2005). Closed-loop flow control based on linear models has a broad development over recent years, as reviewed in (Bagheri and Henningson, 2011; Kim and Bewley, 2007), and experimental applications have shown the feasibility to delay boundary-layer transition in wind tunnel (Fabbiane *et al.*, 2015; Sturzebecher and Nitsche, 2003) and flight tests (Simon *et al.*, 2016).

Most studies fix a sensor-actuator structure (placement and shape) and disturbance type, and move on from this point. When sensor-actuator parameters are fixed, the specific control problem that is being dealt with does not correspond entirely to the main control objective. As the goal is to achieve the best possible way to control instabilities, the sensor-actuator structure is in itself a project variable, even considering that in practical applications there is more flexibility to manipulate the placement than the shapes or mechanisms of sensors and actuators.

The problem of selecting sensors and actuators can be explored in a trial-and-error basis (Belson *et al.*, 2011), but this is clearly inefficient and costly. Optimization techniques for the sensor and actuator placement aiming the control performance have been developed (Chen and Rowley, 2011, 2014); these lead to optimal placement choices, but are not able to explain in physical terms the reason one given placement provides different results from another. The explanation

attempts based on eigenmode analysis (Bagheri *et al.*, 2009b) and sensitivity analysis (wavemaker region) (Giannetti and Luchini; Chomaz) are not able to predict the optimal placement (Illingworth and Oehler, 2018), which indicates that fundamental concepts regarding this aspect of the control problem are still not well understood.

The main objective of this work is to provide concepts and a metric that help to understand the performance of a specific sensor-actuator placement, and its variation as the placement changes. The proposed metric involves sensor and actuator characteristics; its value indicates how close control performance is to full-state feedback, and whenever such performance becomes unsatisfactory, the metric can be explored to indicate directions for improvement. Due to its relevance in practical applications aiming at drag reduction, we restrict here our attention to amplified-type flows with a convective instability, such as the boundary layer Huerre and Monkewitz (1990). To show the approach in canonical settings, we first exemplify the application of the methods to the Kuramoto-Sivashinsky equation, a 1D model problem with dynamics similar to transitional boundary layers. The procedure will then be extended for the Blasius boundary layer Fabbiane *et al.* (2014).

This work is organised as follows. In section 2 we show the methods utilized for the analysis. In section 3 the analysis is made for the model problem and extended to the 2D Blasius boundary layer in section 4. In section 5 the conclusions are presented.

2. Methods

2.1 Basic Equations for Convectively Unstable Flows

The linearized, spatiotemporal evolution of perturbations in fluid flow, with a slowly-diverging base profile, can be categorized in three types (Briggs, 1965): (i) stable, (ii) absolutely unstable and (iii) convectively unstable. The present work deals with convectively unstable flows, such as the Blasius boundary layer. The spatiotemporal behavior of such a flow submitted to an impulsive forcing is as shown in Fig. 1.

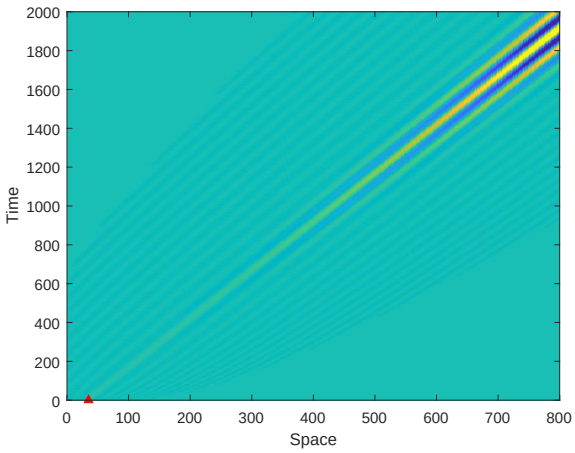

Figure 1: Spatiotemporal response of a convectively unstable flow to an impulsive forcing at ▲.

The system is globally stable, as fluctuations eventually leave the computational domain, leading to an overall decay of perturbation energy. Nevertheless, the propagation of convectively unstable wavepackets in a boundary layer may induce the transition from the laminar to the turbulent flow regime, increasing the overall drag. In order to avoid or mitigate the drag increase, control strategies are applied.

Overall, the control strategies are divided in two classes: passive and active control. In passive control, structural changes are made in the system in order to achieve the transition delay, *e.g.*, different materials, modifications in the surface shape (holes, bumps, *etc*). In active control, a control forcing is applied to the system through an actuator. The control forcing can be either calculated in a predetermined manner (open-loop control) or in real-time, based on sensors measurement (closed-loop control).

In order to be able to apply the linear control methods, the flow must be linearized around an operation point, which, for transition control, is the laminar steady-state solution. Efficient transition control applications are often based on controlling disturbances at upstream regions with amplitude growth in agreement with linear stability theory, which justifies linearization of the governing equations. As a result, we obtain a system of the form

$$\dot{q}(t) = Aq(t) \tag{1}$$

where t is time, A is the discretized, linearized Navier-Stokes operator (the state matrix) and q the flow state, regrouping fluctuations of flow quantities at all considered positions. For active control, Eq. (1) should be supplemented with actuators represented by a B_u operator acting on actuator input, *i.e.*, the control input, designated by $u(t)$. The disturbance can be induced in the linear model in two ways: by imposing an appropriate initial condition $q(0)$, or by supposing a disturbance operator B_d, acting on an external disturbance $d(t)$. In the present case the second option is used.

For closed-loop control, in realistic configurations, one does not have access to all state variables, and it is thus necessary to take measurements in the flow which will be used in the calculation of the control input. The sensors are represented by a C_y operator, acting on sensor measurement $y(t)$. It is generally considered that the sensors measurement is corrupted by noise modelled by $n(t)$ (Bagheri *et al.*, 2009b). The closed-loop control law maps $y(t) \mapsto u(t)$ through a transfer function, such that the control action can be determined based on present and past measurements by the sensors.

Finally, the control strategy aims to achieve a certain goal, which will be represented by an objective variable $z(t)$. In the case of convectively unstable perturbations, the goal is to minimize its energy in a position downstream to the actuator (Fig. 2), represented by the C_z operator; minimization of $z(t)$ thus corresponds to avoiding that large-amplitude disturbances reach downstream positions, which leads to transition delay. The framework for the linear problem becomes thus

$$\begin{cases} \dot{q}(t) = Aq(t) + B_u u(t) + B_d d(t) \\ z(t) = C_z q(t) \\ y(t) = C_y q(t) + n(t) \end{cases} \tag{2}$$

For a discretized system, the operators become matrices. B_d and B_u are often taken as discretizations of spatial functions corresponding to the support of body forces modelling the introduction of disturbance and actuation, respectively. C_y and C_z are also spatial functions related to the extraction of flow fluctuations from a given region in the flow. Further details of the formulation of the problem in input-output form are given by (Bagheri *et al.*, 2009a).

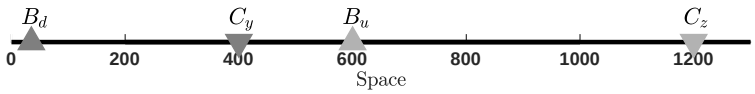

Figure 2: An example of the usual positioning of the inputs (disturbance B_d(▲) and actuator B_u(▲)) and outputs (sensor C_y(▼) and objective C_z(▼)) in a convectively unstable flow.

2.2 $\mathcal{H}_2$ Optimization

The objective in the flow control of convective instabilities is to minimize the energy of the linear convective wavepacket generated by the input disturbance $d(t)$ in order to delay transition to turbulence. As the performance variable z in (2) serves as the representation of downstream fluctuations, the objective is to minimize the energy power of z.

The control approach that fits this objective is the $\mathcal{H}_2$ optimization. Given the exogenous input $w(t) = [d(t) \;\; n(t)]^T$, regrouping introduced disturbance and sensor noise, and the control objective $z(t)$, the controller $H(s)$ internally stabilizes the plant $G(s)$ and optimally minimizes the transfer function $T_{zw}(s)$, *i.e.*, from w to z, according to the $\mathcal{H}_2$ norm (Fig. 3); here a Laplace transform is taken, and s refers to the Laplace variable. This procedure is equivalent to minimize the energy power of z when w is given by white noise, as usually is assumed in flow control problems.

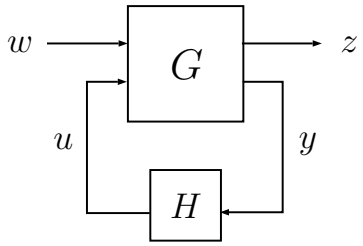

Figure 3: General control configuration.

Suppose d and n in (2) are white-noise disturbances with spectral densities W and V, respectively. An auxiliary objective variable $\tilde{z}$ is defined as

$$\tilde{z}(t) = \begin{bmatrix} Q^{\frac{1}{2}}C_z & 0 \\ 0 & R^{\frac{1}{2}} \end{bmatrix} \begin{bmatrix} q(t) \\ u(t) \end{bmatrix} \tag{3}$$

with positive-definite weight matrices Q and R related to control performance and actuation cost, respectively. The inclusion of the actuation energy in the auxiliary objective variable $\tilde{z}$ has two reasons: First, the inclusion of a positive definite matrix R, penalizing actuation, is required for a nonsingular $\mathcal{H}_2$ optimization problem. Second, in practice the actuator has limitations in the input forcing it can provide and it is desirable to minimize the energy spent by the controller; otherwise, one may arrive at a situation where power spent by actuation is larger than what is saved by closed-loop control. The matrices Q and R are then weights that can be tuned, imposing a trade-off between performance and actuation energy that is, in fact, a necessary project variable.

The Laplace-transformed, open-loop transfer function $G(s)$ (Fig. 3) is given by (Skogestad and Postlethwaite, 2005)

$$G(s) = \left[\begin{array}{c|cc:c} A & B_d W^{\frac{1}{2}} & 0 & B_u \\ \hline Q^{\frac{1}{2}}C_z & 0 & 0 & 0 \\ 0 & 0 & 0 & R^{\frac{1}{2}} \\ \hdashline C_y & 0 & V^{\frac{1}{2}} & 0 \end{array}\right] \tag{4}$$

The $\mathcal{H}_2$ norm of the transfer function T_{zw} is given by

$$\| T_{zw} \|_2^2 = < \tilde{z}^T(\infty)\tilde{z}(\infty) > = < q^T(\infty)C_z^T Q C_z q(\infty) + u^T(\infty)Ru(\infty) > \tag{5}$$

where $\tilde{z}(\infty)$ is the value of $\tilde{z}$ in the steady-state. This is the linear quadratic gaussian (LQG) problem written in the $\mathcal{H}_2$ optimization framework. The solution to this problem is subject to the separation theorem (Åström, 1970), which states that the optimal control strategy can be separated in two parts: a state estimator which provides the optimal estimation of the system state from the measurement of the sensors, known as the Linear Quadratic Estimator (LQE) or Kalman filter, and a linear feedback law which gives the control signal as a linear function of the estimated state, known as Linear Quadratic Regulator (LQR) (Fig. 4).

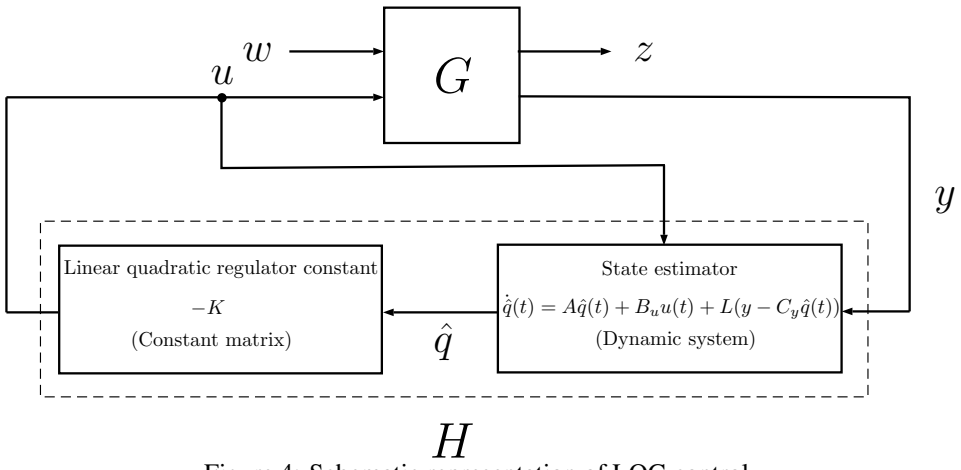

Figure 4: Schematic representation of LQG control.

Given the equivalence between the response to a stochastic forcing and to an impulsive forcing, throughout this work it is assumed the system is submitted to impulsive forcings.

2.3 Actuation Error due to State Estimation Error (γ-metric)

The system dynamics, given by,

$$\dot{q}(t) = Aq(t) + B_u u(t) + B_d d(t)$$

allows an optimal state estimation in the $\mathcal{H}_2$ framework via a Kalman filter, given by

$$\dot{\hat{q}}(t) = A\hat{q}(t) + B_u u(t) + L(y(t) - C_y\hat{q}(t)) \tag{6}$$

where L is a matrix obtained by standard methods involving the solution of a Riccati equation (Skogestad and Postlethwaite, 2005).

The error in the estimation, $e(t) = q(t) - \hat{q}(t)$, has its dynamics given by

$$\dot{e}(t) = (A + LC_y)e(t) + B_d d(t) \tag{7}$$

For the LQG compensator, the control law is given by K times the estimated state, which becomes

$$u(t) \quad = -K\hat{q}(t) = -Kq(t) + Ke(t) = u_{LQR}(t) + u_e(t) \tag{8}$$

where K is the linear quadratic regulator (LQR), u_{LQR} is the actuation law for the LQR problem and u_e is the error in the actuation law due to the estimation error in the LQG problem. Similarly to the Kalman filter L, the optimal K minimizing the objective in Eq. (5) is obtained through the solution of a Riccati equation. When a single control input u is considered, (8) shows that K should be a matrix with dimension equal to the transpose of the state. Hence, the operation $u(t) = -K\hat{q}(t)$ can be seen as an inner product, with the determination of the control by the projection of the estimated state onto the control gains K. Since the state $\hat{q}$ in flow problems corresponds to fluctuations in velocity and/or pressure in contiguous positions in the discretization scheme, the gain K also has an implicit spatial dependence and can be evaluated to determine which regions require an accurate estimation of the state.

As the error of the estimation to an impulsive forcing $d(t) = \delta(t)$ is

$$e_i(t) = e^{(A+LC_y)t}B_d \tag{9}$$

the energy of the error of the actuation law $u_e(t)$ is defined as

$$\gamma(B_u, C_y) = \int_0^{+\infty} (Ke_i(t))^2 dt = \int_0^{+\infty} B_d^T e^{(A+LC_y)^T t}\ K^T K e^{(A+LC_y)t} B_d dt \tag{10}$$

where the actuator B_u determines the gain K and the sensor C_y determines the gain L. The metric γ so defined is the main contribution of the present work, and it will be studied in detail in what follows. The expression (10) can be rewritten as

$$\gamma(B_u, C_y) = Tr(KP_eK^T) \tag{11}$$

where P_e, the covariance of the estimation error, is the solution of the Lyapunov equation

$$(A + LC_y)P_e + P_e(A + LC_y)^T + B_d B_d^T = 0 \tag{12}$$

Since P_e is a Hermitian matrix, it has the eigenvalue-eigenfunction decomposition

$$P_e = \left[\begin{array}{c|c|c} \cdots & \phi_{e_v} & \cdots \end{array} \right] \left[\begin{array}{ccc} \ddots & & \\ & \sigma_{e_v} & \\ & & \ddots \end{array} \right] \left[\begin{array}{c} \vdots \\ \hline \phi_{e_v}^T \\ \hline \vdots \end{array} \right] \tag{13}$$

and the expression (11) can be rewritten as

$$\gamma(B_u, C_y) = \textstyle\sum_v \sigma_{e_v} < \phi_{e_v} | K^T >^2 \tag{14}$$

The value of the γ-metric can thus be regarded as a measure of the extent the estimation error modes ϕ_{ev} are projected on the LQR gain K, weighted by the singular values σ_{cev}.

Sensor and actuator placements are inherently coupled. As a consequence, the sensor does not need to provide a good estimation of all the flow degrees of freedom, but only of those that will in fact be used to determine the control actuation, *i.e.*, the degrees of freedom indicated by the LQR gain K. The γ-metric, in this sense, measures the quality of the estimation where it will be uselful.

From (8), if $u_e(t) = 0$, the error of state estimation does not affect the control problem and its performance will be the same as the one from LQR, which is the best that can be achieved for a given actuator position. So, if $\gamma \to 0$, it means $Ke(t) \to 0$, making the system approach the full-state-feedback performance.

As an overall criteria, a sensor-actuator pair (B_u, C_y) such that

$$\frac{\gamma(B_u, C_y)}{\| K \|^2} \ll 1 \tag{15}$$

provides a control performance that is not significantly degraded by the estimation error.

3. Application to a Model Problem: the Kuramoto-Sivashinsky Equation

3.1 Full-state Feedback (LQR)

Considering the full information problem, *i.e.*, all the degrees of freedom values are available, the system equation becomes

$$\begin{cases} \dot{q}(t) = Aq(t) + B_u u(t) + B_d d(t) \\ z(t) = C_z q(t) \end{cases} \tag{16}$$

As the goal is to minimize the energy power of z, the first question to be answered is if it is possible to find a controller F such that.

$$T_{zd}(s) = C_z(sI - A - BF)^{-1} B_d = 0 \tag{17}$$

The control mechanism in convective instability is the generation of a similar wave with opposite phase, *i.e.*, wave cancellation (Sasaki *et al.*, 2018). Find a controller such that (17) holds is then equivalent to the theoretical possibility of the actuator exactly reproduce the disturbance with opposite phase through state feedback. For the controller calculation, the values of the weights chosen in (4) were $Q = 1$, $V = 10^{-2}$ and $R = 10^{-4}$, so that the control provides the best performance possible. Decreasing the value of R does not improve control performance.

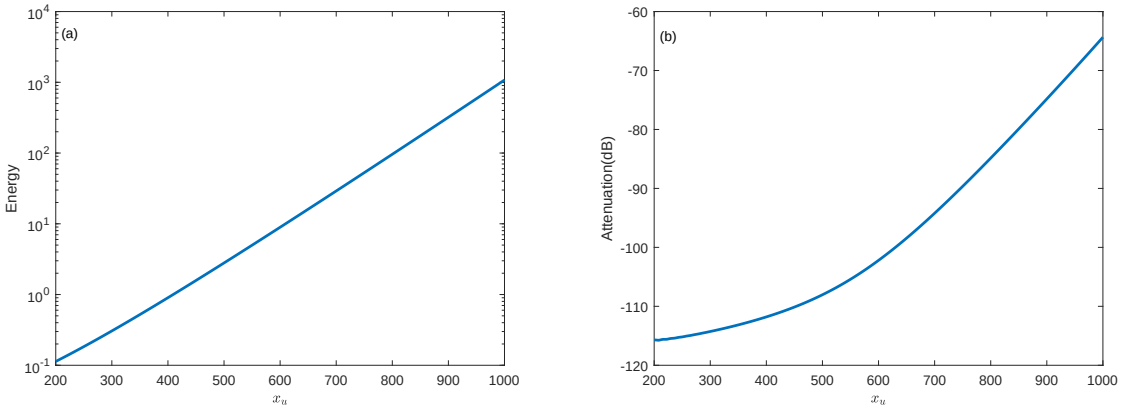

(a) (b)

Figure 5: LQR control: (a) Actuation energy for actuator at position x_u. (b) Energy attenuation at z (16) for actuation at position x_u normalized by the uncontrolled energy.

In Fig. 5a it is shown that the actuation energy increases as the actuator is moved downstream, as expected given the disturbance is amplified as it moves downstream.

In Fig. 5b it is shown that the LQR performance degrades as the actuator is moved downstream. This result suggests that the further the disturbance has developed, the ability of the actuator to reproduce its waveform degrades.

Both results indicate the actuator should be placed as upstream as possible, as the actuator will provide a better attenuation spending less control energy, keeping in mind any disturbance that acts in the flow downstream of the actuator will not be controlled.

3.1.1 LQG Control Performance

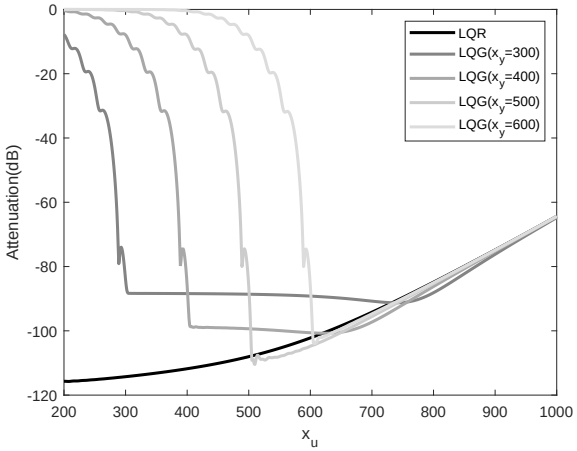

Figure 6: Energy attenuation at z normalized by the uncontrolled energy.

The performances of various control systems are summarised in Fig. 6. Consistently with the results of the γ metric, results indicate as the actuator is placed downstream to the sensor, the performance improves dramatically. For sensor positions $x_y = 300$ and 400, as the actuator is moved further downstream, the performance is dominated by the effect of γ, which then remains almost constant until the degradation of the actuator's ability to reproduce the incoming waveform becomes more prominent and dominates the controlled system performance; this can be seen by the LQG controllers approaching the LQR results, which are solely related to actuator performance. It is worth noting that the better attenuation presented by the LQG compared to the LQR for some sensor/actuators positions may be due to that the error $e(t)$ (Eq. 8) presents a pattern that in fact aids in the control.

The close relationship between γ and control performance is seen in Fig. 8.

For the same cases, the required actuation energy is shown in Fig. 7. The curves have oscillatory shapes when actuators are upstream of sensors, but this occurs in regions of poor performance (compare with figure 11) and is thus not particularly relevant. Once actuators are placed downstream of sensors, the actuation energy becomes quite close to the LQR result, with exponential growth as the actuation is moved downstream. Despite this exponential growth, the performance gain is minimal in the relatively flat portion of the performance curve, seen in Fig. 6. This leads to a similar placement rule to the one proposed in Sec. 3.1 the actuator should be placed downstream of the sensor, upstream enough to reach the relatively flat performance curve (in the γ-dominated zone) or to achieve the best performance (in the actuator degradation-dominated zone).

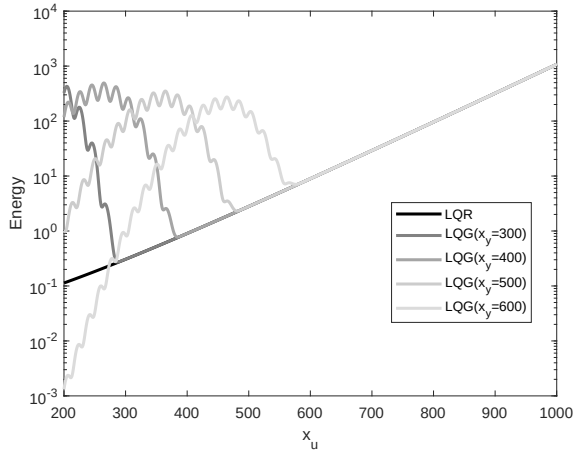

Figure 7: LQG actuation energy for actuator at position x_u.

A further association of control performance with γ is shown in Fig. 8. In Figs. 8 (a) and (b) the sensor position is fixed and actuator placement is varied, and in Figs. 8 (c) and (d) the actuator is fixed and the sensor moves. We notice a strong

similarity between the control performance, shown in Figs. 8 (a) and (c), with the γ-metric shown in Figs. 8 (b) and (d). Attenuation of several orders of magnitude of incoming disturbances occurs when $\frac{\gamma}{\|K\|^2} \ll 1$, and when $\frac{\gamma}{\|K\|^2} \gg 1$ no attenuation occurs. Here this is observed for several sensor/actuator placements, but the value of $\frac{\gamma}{\|K\|^2}$ already indicates if a given placement choice could be significantly improved: low values are associated with performances close to LQR, and values of about 1 show that improvement is possible, indicating also how to enhance performance by a further analysis of the overlap between error modes and LQR gains.

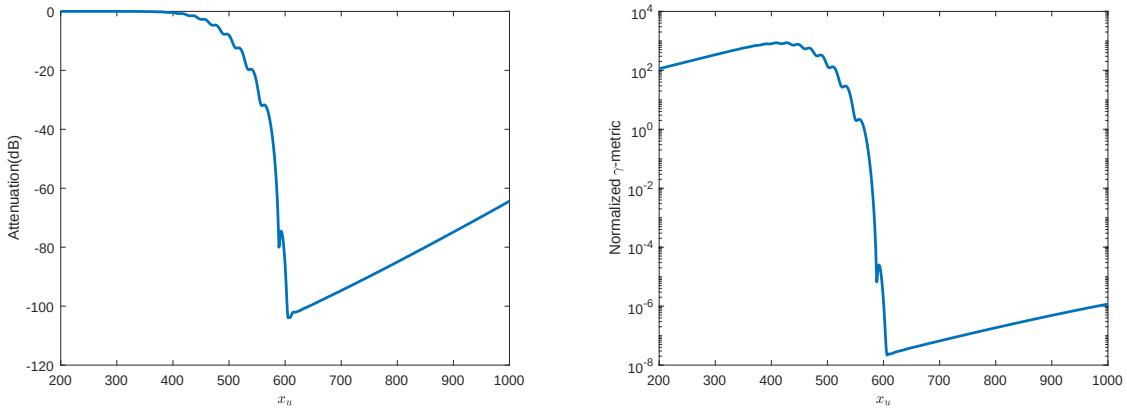

(a) (b)

(a) Energy attenuation at z normalized by the uncontrolled energy, for the sensor fixed at $x_y = 600$ and the actuator at position x_u; and (b) the corresponding γ-metric normalized by $\| K \|^2$.

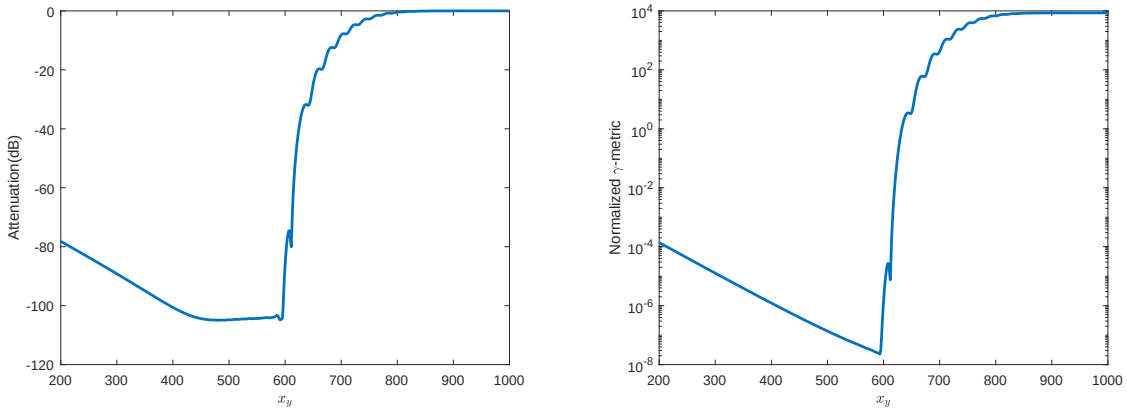

(c) (d)

(c) Energy attenuation at z normalized by the uncontrolled energy, for the actuator fixed at x_u = 600 and the sensor at position x_y; and (d) the corresponding γ-metric normalized by $\| K \|^2$.

Figure 8: Control performance and normalized γ-metric

3.1.2 LQG Performance With Fixed Sensor-Actuator Distance

We have seen that available choices for the sensor-actuator placement lead to control performance dictated by either estimation errors, labelled as γ-dominated region, or dominated by the actuator's degradation; for the latter case, the attenuation follows the LQR performance curve (Fig. 5a).

We study further these two effects on control performance by considering the sensor-actuator placement suggested in Sec. 3.1.1, *i.e.*, downstream of the sensor, but sufficiently upstream. This distance will be assumed to be $x_u - x_y = 10$, and will remain fixed; sensors and actuators will be moved up and downstream maintaining this arrangement, with fixed distance. The results of control performance for LQG are shown in Fig. 9, together with the reference LQR results and the γ metric. For the most upstream position of the sensor/actuator pair ($x_y = 200$, $x_u = 210$) the actuator's degradation is in its lowest level, as shown in Fig. 5b, and one may assume that the performance variation is dictated by the γ variation in this region. To see this, the γ curve is shifted in order to match the LQG performance at position $x_u = 210$, and we observe that it follows closely the performance results for $x_u < 400$. It is seen that the control performance is dictated either by the LQR performance (for a downstream sensor-actuator pair) or by estimation error of the relevant degrees of

freedom for the actuation calculation (for an upstream pair, where the γ effect on performance becomes more significant).

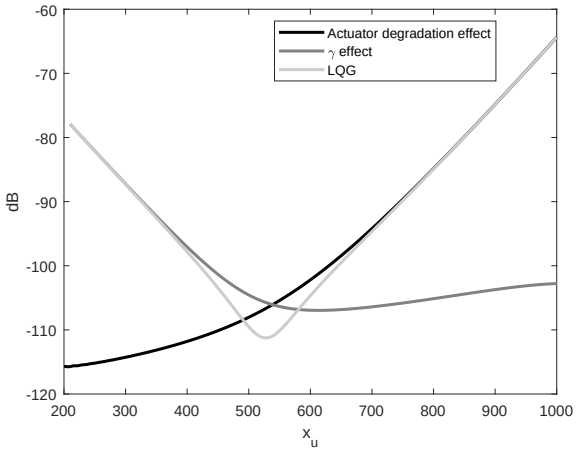

Figure 9: Dominated regions and the LQG performance for $x_u - x_y = 10$.

4. 2D Boundary Layer Results

The simulations of the 2D Blasius boundary layer were carried out with the SIMSON pseudo-spectral solver Chevalier *et al.* (2007). The size of the domain used was $l_x \times l_y = 1000 \times 30$, with a fringe of length $L_f = 200$. Non-dimensional variables are used, considering the free-stream velocity and the inflow displacement thickness as reference velocity and length, respectively. With these definitions, the Reynolds number is 1000. The discretization in the horizontal axis was done through a Fourier series expansion with $n_x = 768$ modes, and through a Chebyshev expansion with $n_y = 101$ as the highest order of the polynomials. The disturbance B_d was placed at $x_d = 35$ and the objective C_z at $x_z = 500$. The actuators are localized volume forcings, as described in Semeraro *et al.* (2013) and the sensors are localized stress sensors. For the positions where the sensor is upstream to the actuator, the weights chosen in (4) were $Q = 1$, $R = 10^2$ and $V = 1$. For the sensor at the position or downstream to the actuator the weights chosen were $Q = 1$, $R = 10^4$ and $V = 10^4$; lower weight values led to controllers destabilising the system.

4.1 γ-metric

A reduced order model was obtained through the POD model reduction (Rowley, 2005). The LQR gain was calculated with the reduced order model for the actuator fixed at $x_u = 350$ and we have recovered to the original physical state using the POD modes; the results are shown in Fig. 10. We observe that the LQR gain K has the overall features of a wavepacket shape downstream of actuator position. We notice also a phase opposition in y, characteristic of Tollmien-Schlichting waves. Besides the dominant wavepacket, the gain K also displays lower amplitude oscillations extendind up and downstream, particularly for the streamwise component u. The γ-metric for the 2D boundary layer, supposing point sensors, was calculated for the whole field. The overall result is shown in Fig. 11, and Fig. 12 shows the metric taken at the station $x = 200$. These results provide a guide to explore sensor positioning and shape. In Fig. 11 are presented the sensor positions able to deliver accurate estimates for the degrees of freedom the actuator needs for the actuation calculation, which are depicted in Fig. 10.

It therefore shows positions where the measurement of the horizontal and vertical components of the velocity of the flow will result in a better control performance. The results for the Blasius boundary layer show that sensors should be placed upstream of the actuator, within the blue region in Fig. 11. Results also show that measurements of both u and v may lead to good estimations of the required degrees of freedom. Exceptions are the nodal positions for u in y, around which there is the cited phase opposition of T-S waves, and the near-wall region for v, as shown more clearly in Fig. 12.

4.2 Control Performance

For closed-loop control of boundary layer the actuator was fixed at position $x_u = 350$ and the position of the sensor was changed, as this allows the use of a single set of POD modes to obtain reduced-order models for all actuator placements. Control laws are then obtained using the reduced-order model, and are subsequently applied to the full-order nonlinear simulation. Results are shown in Fig. 13 and resemble what was shown in Fig. 8(b) for the Kuramoto-Sivashinsky system. The similarity between the shapes of the attenuation curve and the γ metric shows that the criterium proposed in (15), of normalized γ much lower than 1, holds for the 2D Blasius boundary layer: whenever $\frac{\gamma}{\|K\|^2} \ll 1$ closed-loop

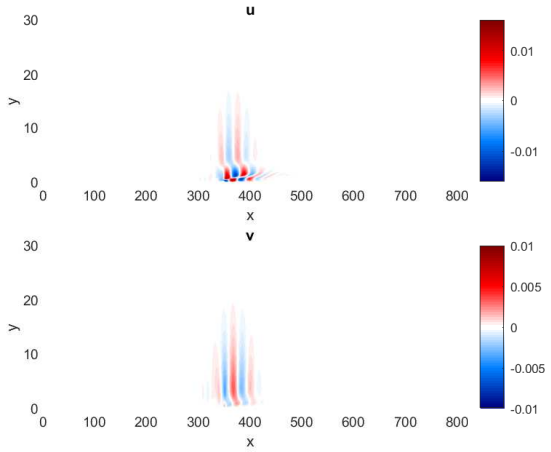

Figure 10: LQR for the 2D boundary layer, recovered using the POD modes, for the actuator at x_u=350.

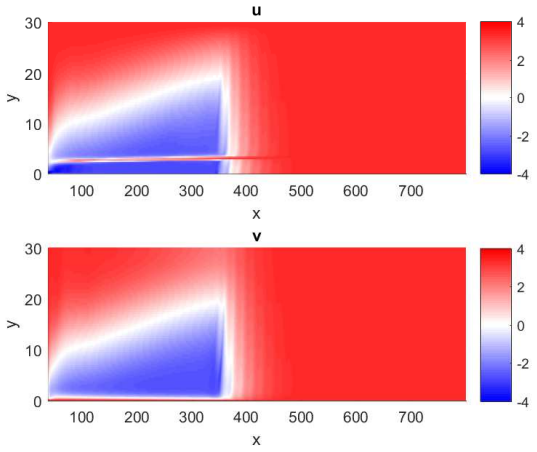

Figure 11: The log_{10} of the normalized γ-metric for the 2D boundary layer for the actuator fixed at x_u=350, supposing pontual sensors. Positions downstream to the disturbance at $x_d = 35$ were excluded from possible sensor positions.

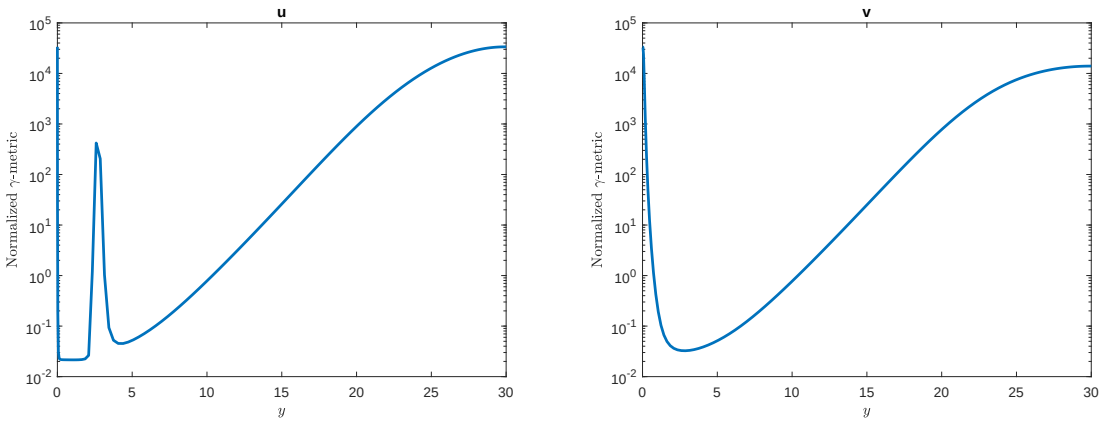

(a) (b)

Figure 12: Cross-section for $x = 200$ of the velocity components (a) u and (b) v in Fig. 11.

control leads to an attenuation of disturbances of several orders of magnitude. Here errors in model reduction also play a role, which may explain the oscillations in Fig. 13 for upstream sensor positions ; however, such oscillations occur around an attenuation of 30dB, and thus all configurations lead to good control performance.

The increase in the γ-metric can be visualized by the spatial superposition of the LQR and the error modes (Fig. 14).

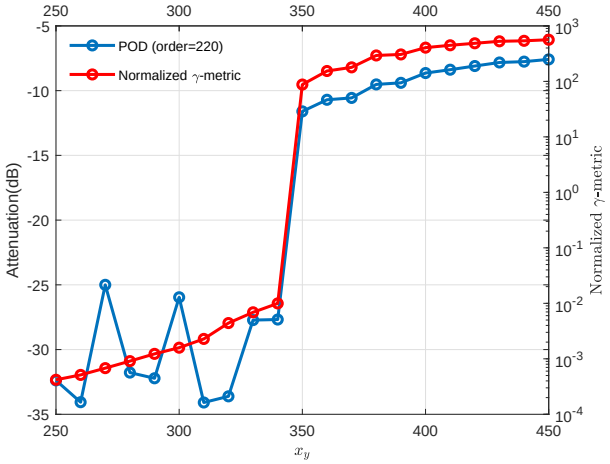

Figure 13: 2D Blasius boundary layer controlled with LQG controllers of order $k = 220$ for the actuator fixed at position $x_u = 350$ and sensor at position x_y, and corresponding normalized γ-metric.

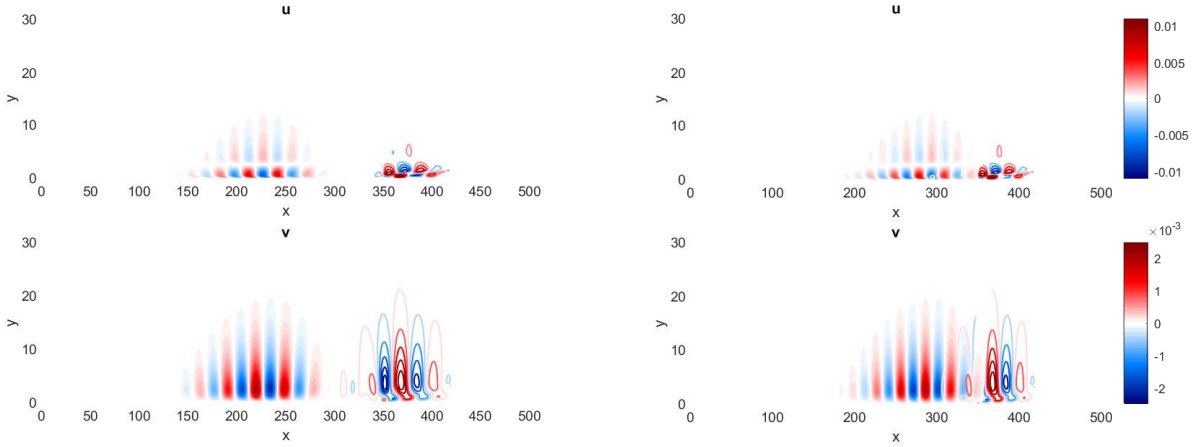

(a) (b)

Figure 14: LQR for the 2D boundary layer in solid lines (Fig. 10) and the first error mode for sensor at position (a) $x_y = 300$ and (b) $x_y = 370$.

In Fig. 14(a), the spatial supports do not overlap, indicating a low value for the γ-metric, as seen in Fig. 13. In Fig. 14(b), the spatial supports overlap, increasing the γ-metric value and degrading the control performance, as seen in Fig. 13. It is worth noting that in the last case, for $x_u = 350$ and $x_y = 370$, the error modes were generated using the weights $R = 10^2$ and $V = 1$; nevertheless, generating the LQG controller using these same weights result in an unstable compensator. It is then necessary to increase the weights ($R = 10^4$ and $V = 10^4$) to obtain a stable compensator, that despite degraded compared to a positioning where the sensor is downstream to the actuator, can still provide around 10dB in attenuation, as seen in Fig. 13.

Similarly to the results in Fig. 9, the distance between the sensor and actuator was fixed such that $x_u - x_y = 100$ and the control performance evaluated for the different positions of the sensor-actuator pair. Results are shown in Fig. 15. It is reasonable to assume the error due to the model reduction dominates the system performance, such that the characteristic regions discussed in Sec. 3.1.2 do not appear in the boundary layer simulation. In all cases an attenuation of about three orders of magnitude is obtained by the controller, and the decrease of model-reduction errors might lead to even better performances.

5. Conclusion

The role of the sensor-actuator placement as a project variable cannot be neglected, as implied by the model problem and shown in a boundary layer simulation. The concepts discussed and the proposed γ-metric explain why and to what extent certain pairs of sensors and actuators are more effective than others.

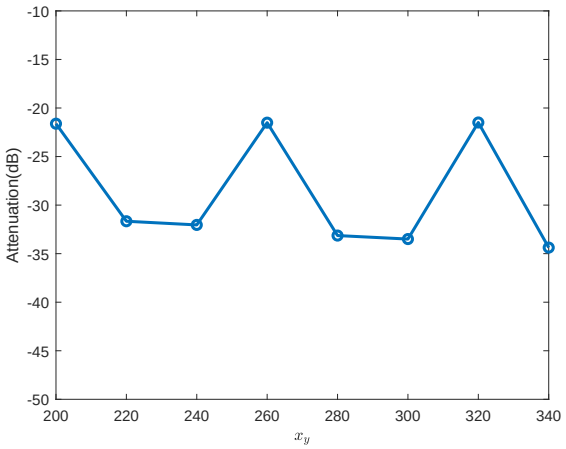

Figure 15: 2D Blasius boundary layer controlled with LQG controllers of order $k = 220$. The distance $x_u - x_y = 100$ is fixed and $x_z = 500$.

From the results obtained, a strategy for the sensor-actuator positioning can be proposed. We start by fixing an actuator position *a priori*. Given the ubiquitous need for model reduction in flow control problems, the well established POD model reduction will provide a single set of modes that can be used to obtain the reduced order model for any possible sensor placement. With the reduced-order models, the closed-loop performance can be evaluated through the value of $\frac{\gamma}{\|K\|^2}$, as described in Sec. 2.3 values much lower than 1 indicate good closed-loop performance, close to full-state feedback, whereas values of order 1 or higher show that significant estimation errors occur at regions with high control gains. In the case of unsatisfactory performance, the error modes can provide an intuitive indication of where to move the sensor relative to the actuator, as it is desirable that the overlap between the LQR gains and the estimation error modes is as small as possible.

Such error modes, with their intuitive interpretation, can be a valuable aid in the exploration of more complex fluid flow configurations and instabilities, as 3D boundary layers, crossflow and bypass transition, as the efficient placement of sensors and actuators is less straightforward than in a 2D boundary layer, with more possibilities involving also the span. The proposed techniques may also be valuable for more complex geometries with similar amplified behaviour, such as a backwards-facing step (Barbagallo *et al.*, 2012).

6. ACKNOWLEDGEMENTS

The authors acknowledge Capes for the financial support provided.

7. REFERENCES

Åström, K.J., 1970. *Introduction to Stochastic Control Theory*. Academic Press, New York and London.

Bagheri, S., Brandt, L. and Henningson, D.S., 2009a. "Input-output analysis, model reduction and control of the flat-plate boundary layer". *Journal of Fluid Mechanics*, Vol. 620, pp. 263–298.

Bagheri, S. and Henningson, D., 2011. "Transition delay using control theory". *Philosophical Transactions on The Royal Society*.

Bagheri, S., Henningson, D., Hoepffner, J. and Schmid, P., 2009b. "Input-output analysis and control design applied to a linear model of spatially developing flows". *Applied Mechanics Reviews*, Vol. 62.

Barbagallo, A., Dergham, G., Sipp, D., Schmid, P.J. and Robinet, J.C., 2012. "Closed-loop control of unsteadiness over a rounded backward-facing step". *Journal of Fluid Mechanics*, Vol. 703, p. 326–362. doi:10.1017/jfm.2012.223.

Belson, B., Semeraro, O., Rowley, C., Pralits, J. and Henningson, D., 2011. "Robustness of reduced-order observer-based controllers in transitional 2d blasius boundary layers".

Briggs, R.J., 1965. *Electro-beam interaction with plasmas*. MIT, Cambridge, MA.

Chen, K.K. and Rowley, C.W., 2011. "$\mathcal{H}_2$ optimal actuator and sensor placement in the linearised complex ginzburg-landau system". *Journal of Fluid Mechanics*, Vol. 681.

Chen, K.K. and Rowley, C.W., 2014. "Fluid flow control applications of $\mathcal{H}_2$ optimal actuator and sensor placement". *American Control Conference*.

Chevalier, M., Schlatter, P., Lundbladh, A. and Henningson, D., 2007. "A pseudo-spectral solver for incompressible boundary layer flows". Technical report.

Chomaz, J.M., ???? "Global instabilities in spatially developing flows: non-normality and nonlinearity". *Journal of Fluid Mechanics*, Vol. 37.

Fabbiane, N., Semeraro, O., Bagheri, S. and Henningson, D., 2014. "Adaptive and model-based control theory applied to convectively unstable flows". *Applied Mechanics Reviews*, Vol. 66.

Fabbiane, N., Simon, B., Fischer, F., Grundmann, S., Bagheri, S. and Henningson, D., 2015. "On the role of adaptivity for robust laminar flow control". *Journal of Fluid Mechanics*, Vol. 767.

Giannetti, F. and Luchini, P., ???? "Structural sensitivity of the first instability of the cylinder wake". *Journal of Fluid Mechanics*, Vol. 581.

Huerre, P. and Monkewitz, P.A., 1990. "Local and global instabilities in spatially developing flows". *Annual Review of Fluid Mechanics*, Vol. 22, No. 1, pp. 473–537.

Illingworth, S.J. and Oehler, S.F., 2018. "Sensor and actuator placement trade-offs for a linear model of spatially developing flows". *Journal of Fluid Mechanics*, Vol. 854.

Kim, J. and Bewley, T., 2007. "A linear systems approach to flow control". *Annual Review of Fluid Mechanics*, Vol. 39, pp. 383–417.

Rowley, C., 2005. "Model reduction for fluids, using balanced proper orthogonal decomposition". *Int. J. on Bifurcation and Chaos*.

Sasaki, K., Morra, P., Fabbiane, N., Cavalieri, A., Hanifi, A. and Henningson, D., 2018. "On the wave-cancelling nature of boundary layer flow control". *Theoretical and Computational Fluid Dynamics*.

Schrauf, G., 2005. "Status and perspectives of laminar flow". *The Aeronautical Journal*.

Semeraro, O., Bagheri, S., Brandt, L. and Henningson, D.S., 2013. "Transition delay in a boundary layer flow using active control". *Journal of Fluid Mechanics*, Vol. 731, p. 288–311. doi:10.1017/jfm.2013.299.

Simon, B., Fabbiane, N., Nemitz, T., Bagheri, S., Henningson, D.S. and Grundmann, S., 2016. "In-flight active wave cancelation with delayed-x-lms control algorithm in a laminar boundary layer". *Experiments in Fluids*, Vol. 57, No. 10, p. 160.

Skogestad, S. and Postlethwaite, I., 2005. *Multivariable Feedback Control*. Wiley, London, 2nd edition.

Sturzebecher, D. and Nitsche, W., 2003. "Active cancellation of tollmien–schlichting instabilities on a wing using multi-channel sensor actuator systems". *International Journal of Heat and Fluid Flow*, Vol. 24.

8. RESPONSIBILITY NOTICE

The authors are the only responsible for the printed material included in this paper.